Microdomains Shift and Rotate in the Lateral Wall of Cochlear Outer Hair Cells

Rei Kitani,[†△] Channy Park,[†△] and Federico Kalinec[†‡*]
[†]Division of Cell Biology and Genetics, House Research Institute, Los Angeles, California; and [‡]Departments of Cell & Neurobiology and Otolaryngology, Keck School of Medicine, University of Southern California, Los Angeles, California

ABSTRACT Outer hair cell (OHC) electromotility, a response consisting of reversible changes in cell length and diameter induced by electrical stimulation, confers remarkable sensitivity and frequency resolution to the mammalian inner ear. Looking for a better understanding of this mechanism, we labeled isolated guinea pig OHCs with microspheres and, using high-speed video recording, investigated their movements at the apical, mid, and basal regions of osmotically and electrically stimulated cells. After hypoosmotic challenge, OHCs shortened and their diameter increased, with microspheres moving always toward the central plane; iso-osmolarity returned OHCs to their original shape and microspheres to their original positions. Under electrical stimulation, microspheres exhibited robust movements, with their displacement vectors changing in direction from random to parallel to the longitudinal axis of the cells with peak reorientation speeds of up to 6 rad/s and returning to random after 5 min without stimulation. Alterations in plasma-membrane cholesterol levels as well as cytoskeleton integrity affected microsphere responses. We concluded that microspheres attach to different molecular microdomains, and these microdomains are able to shift and rotate in the plane of the OHC lateral wall with a dynamics tightly regulated by membrane lipid composition and the cortical cytoskeleton.

INTRODUCTION

Cell membranes contain a number of organized domains of different composition, size, lifetime, and functionality. Domains have been classified by size into shells, complexes, and clusters (<10 nm), nanodomains (between 10 and 100 nm), and microdomains (>100 nm) (1). Because of their size, microdomains might have properties different from those of smaller structures and be more stable. In addition, specific proteins link sets of microdomain molecules to associated cytoskeletal structures (membrane skeleton) (2). The combination of plasma membrane, membrane skeleton, and linkers could be considered a single, three-layered structure with general properties that are more than the simple sum of the particular properties of each layer (1–3).

Outer hair cells (OHCs) are cylindrical, with a near constant diameter of ~8 μm and length ranging from 20 to 90 μm. They respond to a variety of stimuli by changing length and diameter in an actin-dependent process known as OHC slow motility. In addition, they are able to elongate and shorten at frequencies of up to 100 kHz—and presumably beyond that—after electrical stimulation (4,5). This motile response, usually referred to as OHC electromotility, is a crucial component of the cochlear amplifier, the active process that enhances sensitivity and frequency discrimination in the mammalian inner ear (6–11).

Studies from different laboratories along the last 20 years have provided convincing support for the idea that OHC electromotility is most likely associated with the concerted conformational change of hundreds of thousands of plasma-membrane-embedded motor molecules identified as the protein prestin (12–14). Except for a narrow band at the apex and a basal cup wrapping the infranuclear portion of the cells, dense clusters of prestin and other associated proteins cover the OHC lateral plasma membrane (15–18). The operating voltage range and sensitivity of prestin differ locally, indicating the presence of functional motor microdomains within the OHC lateral plasma membrane (19). Underlying the lateral plasma membrane, and connected to it by thousands of 25-nm-long linkers known as pillars, is a membrane skeleton composed of longer actin filaments cross-linked by shorter spectrin tetramers organized in microdomains of up to 10 μm^2 (20–22). The combination of this particular cytoskeleton arrangement with f-actin inextensibility and spectrin elasticity would provide a vectorial component to the forces generated by prestin molecules in the plasma membrane by harnessing them in the direction perpendicular to the actin cables (20). It is important to note that the angular distribution of cytoskeletal microdomains, as reported by electron microscopy studies (20), is similar to and congruent with the axial diffusion angle of lipids measured by fluorescence recovery after photobleaching (23) and the angular distribution of fluorescent marker displacement vectors in the plasma membrane of

Submitted June 6, 2012, and accepted for publication November 29, 2012.

[△]These authors contributed equally to this work.

*Correspondence: fkalinec@hei.org

Rei Katani's present address is Department of Otolaryngology, Head and Neck Surgery, Graduate School of Medicine, Chiba University, 1-8-1 Inohana, Chuo-ku, Chiba 260-8670, Japan.

Editor: Michael Edidin.

0006-3495/13/01/0008/11 $2.00

http://dx.doi.org/10.1016/j.bpj.2012.11.3828

electrically stimulated cells (24), suggesting a significant influence of the membrane skeleton in the dynamics of the OHC plasma membrane.

In previous publications, we provided a general description of OHC motility in response to osmotic challenges (25,26) and electrical stimulation (25–28). Here, we use polystyrene and carboxylated microspheres (MS) as membrane markers and high-speed video recording to perform a detailed analysis of the local responses of the lateral wall of electrically and osmotically stimulated OHCs. Our results suggest that the lateral wall of guinea pig OHCs consists of discrete structural microdomains that can move relative to each other and change their orientation with respect to the cell axis in both the presence and absence of an external electrical field.

MATERIALS AND METHODS

Isolation of OHCs

Temporal bones were obtained from young albino guinea pigs (*Cavia porcellus*, 200–300 g) of either sex, euthanized with CO_2 according to procedures approved by House Research Institute's Institutional Animal Care and Use Committee. OHCs, isolated as described in the literature (27,28), were transferred to glass-bottomed experimental dishes containing L-15 medium with 25 mM HEPES (Sigma, St. Louis, MO), observed with Nomarski differential interference contrast (DIC) optics on an Axiovert 135TV inverted microscope with a 63×/1.2 C-Apochromat objective (Zeiss, Thornwood, NY), and used within 2 h after isolation. Osmolarity was measured with a freezing-point osmometer (μOsmette 5004, Precision Systems, Natick, MA), and adjusted to 305–310 mOsm with D-glucose or distilled water.

Microsphere labeling

Polystyrene and, in a single experiment, carboxylated MS 0.5 μm in diameter (Polybead Microspheres, Polysciences, Warrington, PA), diluted 1:1000 in L-15, were used as plasma membrane markers (18,29,30). When added to cell suspensions, MS attached tightly and randomly to the surface of the plasma membrane of every cell type in the samples (Fig. 1).

Osmotic stimulation

OHCs suspended in 305–310 mOsm L-15 were osmotically challenged by adding distilled water through a 40-μm-tip-size glass pipette placed ~300 μm away from the base of the cells. After stopping water delivery, the osmolarity of the medium in the immediate neighborhood of the cells slowly returned to initial values and the cells to their initial shape. The amplitude and direction of MS movements were measured every 10 s as long as stimulated cells first shortened and then elongated after stimulation. In a particular experiment, as described in the text, we decreased medium osmolarity and increased cell turgor by adding 10 μL of distilled water directly to the cell suspension (100 μL).

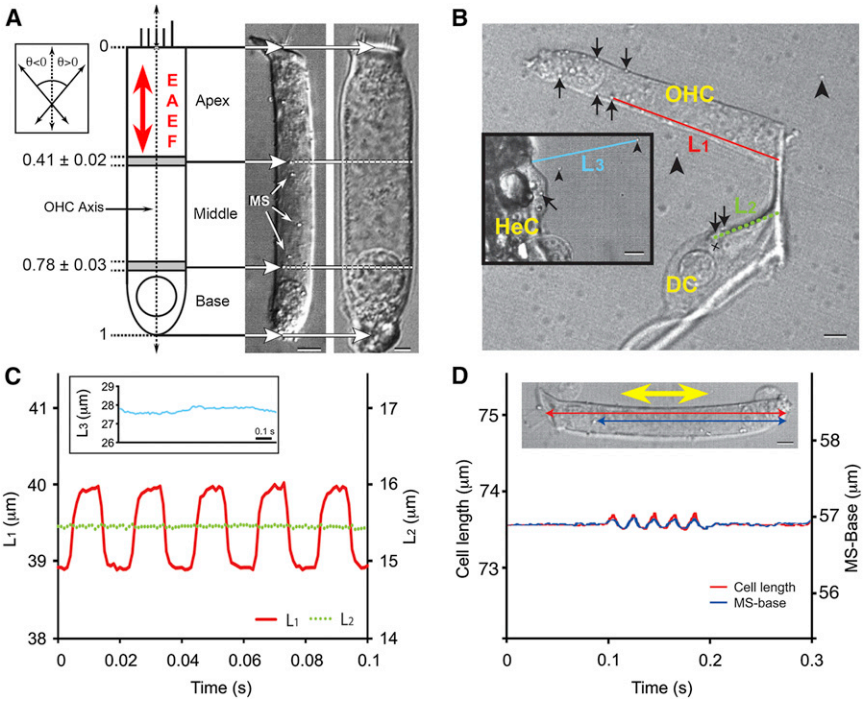

FIGURE 1 MS are reliable indicators of OHC motility. (*A*) Schematic diagram of an OHC showing the three arbitrary regions used for length measurements, the direction of the EAEF (*red arrow*), and two OHCs, one long and the other short, at different scales. In OHCs >50 μm long (*left*) the basal region included the infranuclear, nuclear, and part of the supranuclear region of the cells (scale bar, 6 μm); in OHCs <50 μm long (*right*) the basal region included only the infranuclear and part of the nuclear region (scale bar, 2 μm). (*Inset*) Direction of MS trajectories was defined as the angle (θ) between the line connecting the initial and final position of the MS and the cell's longitudinal axis. (*B*) (DIC) image showing an OHC and a Deiters cell (*DC*) with MS attached to their plasma membranes (*arrows*). Free MS are indicated with arrowheads (scale bar, 5 μm). (*Inset*) DIC image of an isolated Hensen cell (HeC) with an attached MS (*arrow*) and free MS (*arrowheads*) in the neighborhood. L_1 and L_2 indicate the distance vectors from MS attached to the OHC and DC plasma membranes, respectively, to the apices of those cells; L_3 is the distance vector from a free MS to the surface of the HeC (scale bar, 5 μm). (*C*) When the OHC in *B* was stimulated with an EAEF parallel to its longitudinal axis, robust changes in L_1 length (amplitude ~1 μm, *red trace*) were observed as we monitored the electrical signal cycle by cycle. This change of ~2.5% of the L_1 total length (~39.5 μm) is identical to the typical electromotile amplitude of OHCs exposed to an EAEF (28). In contrast, no changes in L_2 (*green trace*) were observed in the Deiters cell shown in *B* for any orientation of the EAEF. (*Inset*) Movement of the free MS depicted in the inset in *B* was also unaffected by the EAEF. Small changes in L_3 (*blue*) were not correlated with electrical stimulation and were probably associated with Brownian movement. (*D*) Incubation of the OHC depicted in the inset with 3 mM Gd^{3+} decreased both electromotile amplitude (*red*) and MS displacement (*blue*) in a proportional way, suggesting that MS displacement was solely associated with OHC motility. The yellow arrow in the inset indicates the direction of the EAEF.

Electrical stimulation

External alternate electrical field

A full description of the equipment and procedures is available in the literature (27,28). Briefly, suspended OHCs were placed in the experimental dish between two silver wire electrodes ($\phi = 0.25$ mm) with a tip distance of 0.8 mm. An 8-V/cm external alternate electrical field (EAEF) was applied between electrodes as 50-Hz bursts of square wave pulses (100 ms on/off). Cell longitudinal axes were kept parallel to the applied EAEF by rotating the recording chamber. Illumination provided by a light-emitting-diode light source (High Power LED System-36AD3500, Lightspeed Technologies, Campbell, CA), electrical stimulation, and image capture were digitally synchronized by control circuitry and software developed by House Research Institute's Engineering Core (27,28).

Whole-cell patch clamp

Patch electrodes were made from borosilicate capillary glass (G-1.5, Narishige, Tokyo, Japan) using a P-97 micropipette puller (Sutter Instruments, Novato, CA). Continuous perfusion of an external solution consisting of L-15 adjusted to 305–310 mOsm with distilled water was provided at a rate of 0.3 mL/min using a syringe pump. Intrapipette solution was composed of 150 mM KCl, 1 mM MgCl2, 0.1 mM EGTA, 2 mM ATP-Mg, 0.1 mM GTP-Na, and10 mM HEPES, with pH adjusted to 7.2 with Tris. The resistance between the patch electrode filled with this solution and the bath solution was 3–6 MΩ. Unless otherwise stated, each OHC was electrically stimulated only once for a 3-s period.

Drug exposure

Cholesterol water-soluble bioreagent (CWS; 1 mM, Sigma) and methyl-β-cyclodextrin (MbCD, 0.5 mM, Sigma) were used for loading and depleting cholesterol, respectively, in the plasma membrane (31), and membrane-permeable ROCK inhibitor Y-27632 (5μM, Sigma) was used to investigate the role of the OHC cytoskeleton (7). OHCs were incubated with these drugs dissolved in L-15 medium for 15 min before the experiments. Gadolinium (Gd^{3+}; 3 mM, Sigma), which was used as a blocker of OHC motility (32,33), was added to an extracellular solution containing (in mM) 140 NaCl, 5 KCl, 2 $CaCl_2$, 1 $MgCl_2$, 10 glucose, and 10 HEPES, with pH adjusted to 7.4 with Tris-OH and osmolarity to 305–310 mOsm with D-glucose since Gd^{3+} is not soluble in L-15. Isolated cells were incubated in this solution for 3 min before electrical stimulation.

Measurement criteria

We defined three regions in OHC images roughly corresponding to the apical 40%, the mid 40%, and the basal 20% of the cell's body length (Fig. 1 *A*). MS localized at the boundaries of these regions were used for measurement of changes in length in electrically stimulated cells. Thus, electrically induced changes in the distance between the cuticular plate and MS in the first 0.41 ± 0.02 boundary are referred to as electromotile amplitude in the apical region, decrease in the distance between MS localized in different boundary zones as decrease in midregion length, etc. Angles were always measured with respect to the OHC longitudinal axis (Fig. 1 *A*, *inset*) and, as shown in Fig. S1 and Movie S1 in Supporting Material, the software automatically followed MS movements, recording and storing, frame by frame, the coordinates of MS trajectories and those of two spots at the extreme base and apex of each OHC that defined its longitudinal axis.

Data handling

Images of isolated OHCs were captured in AVI format at 1000 frames/s (fps) using the ultra-high-speed Photron Fastcam X 1024 PCI camera (Photron USA, San Diego, CA). Cell images were analyzed off-line using ProAnalyst software (Xcitex, Cambridge, MA) and further processed using Excel software (Microsoft, Redmond,WA) (27,28). Statistical analysis, including analysis of variance, contingency, and nonlinear regression techniques, were performed using JMP 9 software (SAS Institute, Cary, NC) and $p \leq 0.05$ as the criterion for statistical significance. Curve fitting was automatically performed using SigmaPlot 11 (Systat Software, San Jose, CA).

RESULTS

MS are reliable indicators of OHC motility

We recorded free MS and MS-labeled cells in the absence of any kind of stimulation for periods of up to 30 min, and with continuous electrical stimulation for up to 3 s (Fig. 1, *B* and *C*). The movement of free MS was not affected by the presence or absence of an EAEF (Fig. 1 *B*, *inset*), and those attached to nonmotile auditory cells were either immotile or their movements were below our limit of detection (Fig. 1, *B* and *C*). MS attached to OHCs, in contrast, were motionless in the absence of electrical stimulation but followed, cycle by cycle, the changes in cell length induced by the EAEF (Fig. 1, *B* and *C*). Incubation of MS-labeled OHCs with 3 mM Gd^{3+}, a nonselective cation-channel blocker known to inhibit OHC electromotility (28), decreased both OHC electromotile amplitude and MS displacement in a proportional manner, suggesting that MS are reliable indicators of OHC motility (Fig. 1 *D*).

Movement of OHC-attached MS in response to osmotic challenge

When a small amount of distilled water was delivered to the basal pole of MS-labeled OHCs, they shortened and their diameter increased; once water delivery stopped, cells slowly recovered their original shape. These changes in cell shape were associated with positional shifts of the MS in the OHC lateral wall (Fig. S2 *A*). By measuring amplitude and direction of MS movements, we found that MS displacement at the apical and basal regions was nearly parallel to the OHC longitudinal axis, whereas those of MS in the midregion were shorter and mostly lateral (Fig. S2, *A–C*). Points representing minimum displacement and maximum angle defined a central plane, presumably containing the center of mass of the cells, which our results placed at a normalized distance of 0.58 from the OHC cuticular plate (Fig. S2, *B* and *C*). Most important, after stimulation, cells slowly recovered their initial shape and MS returned to their original positions, suggesting that MS movements were associated with a coordinated reorganization of plasma-membrane molecules to accommodate changes in cell shape.

Since the movement of MS on the 3D cylindrical cell surface is projected onto a 2D image on the computer screen, measured values are equal to or smaller than actual angles and magnitudes of MS trajectories, with differences

in the radial component increasing for MS closer to the edges of the cell. We performed the corrections and found that they were smaller than the differences between the three regions under study and did not affect the interpretation of the data.

Movement of OHC-attached MS in response to an EAEF

We measured slow and fast motile responses in the apical, mid, and basal regions of electrically stimulated OHCs (Fig. 2). OHCs underwent a total length reduction (slow motility) of ~2% in 3 s. The apical region and midregion began to shorten ~0.4 s after stimulation and continued to shorten at a near-constant rate for the duration of the experiment. Length changes in the basal region, in contrast, were significantly less pronounced and only became evident 0.8 s after the onset of stimulation (Fig. 2 *A*). Electromotile amplitude, on the other hand, was initially greatest at the apex, whereas the movement of the basal region remained nearly constant for the duration of the experiment. Interestingly, in the midregion of the cells, electromotile amplitude increased rapidly for ~0.5 s and then slowed down, approaching apical values (Fig. 2 *B*). Using constrained nonlinear regression techniques we calculated that electromotile amplitude reached a plateau at 0.86 ± 0.18 s in the apical region, at 1.58 ± 0.28 s in the midregion, and at 0.33 ± 0.03 s in the basal region. Thus, we estimated that OHCs required ~1.6 s to reach their greatest electromotile amplitude, a value consistent with previously reported data (28).

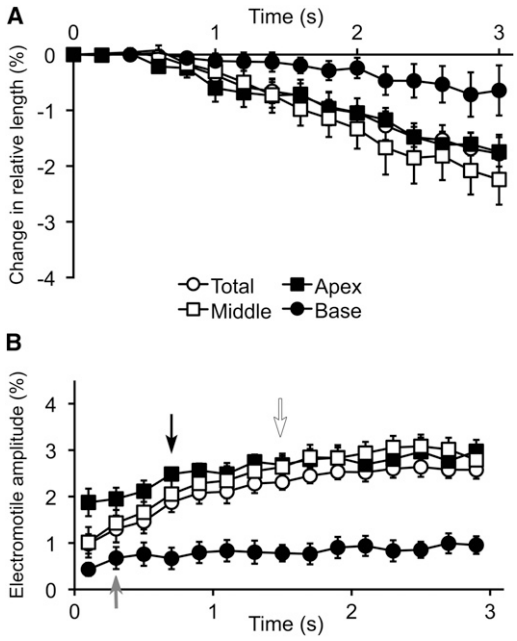

FIGURE 2 Changes in OHC length and electromotile amplitude are region-dependent. Electrically stimulated OHCs (n=7) showed slow motile as well as electromotile responses. (*A*) Slow motile responses resulted in sustained contraction at a rate significantly higher at the apical and mid regions than at the basal portion of the cells. (*B*) Electromotile amplitude was initially higher in the apical than in the mid region of the cells, but both responses became undistinguishable after the first second of stimulation. The basal region, in contrast, showed a reduced response. Electromotile amplitude in the apical region reached a plateau at 0.86 ± 0.18 s (*black arrow*), 1.58 ± 0.28 s in the midregion (*open arrow*), and 0.33 ± 0.03 s in the basal region (*gray arrow*).

EAEF-induced MS movements change direction with time

The observed increase in electromotile amplitude with time prompted us to more closely examine EAEF-induced MS movements. We found that MS showed variable trajectories between the extreme vertices of their movements (Movie S1). In some cases, they were elliptical, becoming narrower as the orientation became axial, and at other times, they were straight or jagged lines. Although the vector determined by the extreme vertices of the trajectory misses some of the richness in the actual movement, it provides a simpler and clearer way to analyze potential changes in the direction of the MS movement. Looking at this vector, we found that MS movement exhibited wide angular dispersion at the onset of stimulation, with no statistical difference between regions (Fig. 3 *A*). During stimulation, the direction of MS movement became increasingly aligned with the cell's longitudinal axis and the electrical field, which were always parallel (Fig. 3, *B* and *C*), and by 3 s of continuous stimulation, most displacement vectors were aligned with them (Fig. 3 *D*). It is important to mention that EAEF-induced effects were reversible. When OHCs were given a second electrical stimulation after a rest period of 5 min, MS movements in every cell region showed increased angular dispersion (Fig. 3 *E*), with 13 of 45 MS movements having angles $>10^{\circ}$ with respect to cell axes compared with only 3 of 45 at 3 s ($P \leq 0.01$; compare Fig. 3, *D* and *E*). Based on these observations, we speculated that MS would be attached to microdomains that were capable of rotating in the plane of the OHC lateral wall to align with the longitudinal axis and could return to random orientations in the absence of external stimulation.

We measured the average reorientation speed of these microdomains, defined as the maximum change in the angle of the MS displacement vectors divided by the time required for completing it, and found significantly lower values in the midregion than in the apical or basal regions of the cells (Fig. 4 *A*), although peak values were similar in all three regions (Fig. 4 *B*). Since the projection of the cylindrical surface of the OHCs onto the computer screen makes the displacement angles for MS with respect to the cell axis smaller than the actual angles, the measured values should be considered low estimates of the reorientation parameters.

To investigate whether microdomain reorientation was affected by changes in OHC turgor, we performed a similar study on osmotically challenged MS-labeled OHCs. Rather

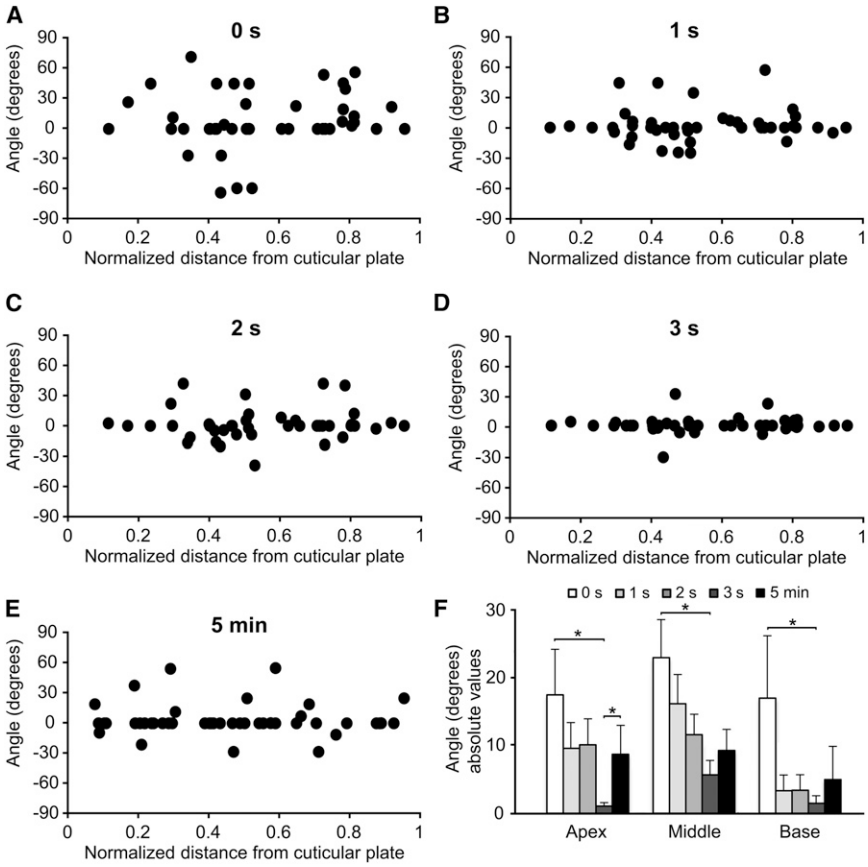

FIGURE 3 The EAEF induces reorientation of MS displacement vectors. (*A*) In response to the initial electrical pulse (0 s), MS (n = 45) moved in different directions (average of absolute angles with respect to the longitudinal axes of the cells: basal region, 16.9 ± 10.6°, midregion, 22.9 ± 5.0°, apical region, 17.4 ± 6.6°; cell average, 20.4 ± 3.7°). (*B*) After 1 s of continuous stimulation, many MS vectors became aligned with the cell axes: basal region, 3.3 ± 2.2°, midregion, 16.1 ± 4.2°, apical region, 9.6 ± 3.7°; cell average, 12.4 ± 2.7°. (*C*) After 2 s, changes in direction were less pronounced than before: basal region, 3.5 ± 2.2°, midregion, 11.6 ± 3.0°, apical region, 10.1 ± 3.8°; cell average, 10.1 ± 2.1°. (*D*) At 3 s, most of the displacement vectors were aligned with the cell axes: basal region, 1.6 ± 1.1°, midregion, 5.8 ± 2.1°, apical region, 1.2 ± 0.5°; cell average, 3.8 ± 1.2°. (*E*) After a rest period of 5 min, the alignment of MS displacement vectors with the cell axes was mostly lost: basal region, 5.0 ± 4.9°, midregion, 9.3 ± 3.1°, apical region, 8.7 ± 4.9°; cell average, 8.6 ± 2.4°. (*F*) Summary of results, showing that most of the MS displacement vectors (in absolute values) reoriented in the first second of stimulation and that the alignment observed at 3 s is lost after 5 min without stimulation, particularly at the apical region. *p ≤ 0.05.

than using the previously described approach of delivering a small amount of distilled water to the basal pole of the cells, which has a transient effect, we decreased the osmolarity of the whole experimental sample by adding distilled water directly to the cell suspension. The results (Fig. S3) indicated that an increase in cell turgor does not affect microdomain reorientation or reorientation speed. This experiment had two important bonuses. Addition of water resulted in the displacement of every free-floating cell in the suspension, and performing measurements on cells immediately after their intentional displacement provided us with further confirmation that they were not attached to the floor of the experimental chamber, a condition that could affect the interpretation of our results. Most important, electromotile amplitude in these cells increased over time just as in previous experiments (Fig. S4). Compare with Fig. 2 *B*), suggesting that cell's turgor is not a major contributor to this response either.

The observations that microdomains change their orientation in the presence and absence of an EAEF, and that this reorientation was not significantly affected by changes in OHC turgor, did not rule out the possibility of an EAEF-associated artifact. Therefore, we investigated whether MS movements change direction with time in whole-cell patch-clamped OHCs. After several unsuccessful attempts, because polystyrene MS clustered on the patch pipette and the patch-clamped OHC interfering with the experiment, we switched to carboxylated MS, which did not show this behavior (18). As shown in Fig. 5 (see also Fig. S5 and Movie S2), microdomains also reorient after whole-cell patch-clamp electrical stimulation, increasing their alignment with the longitudinal axes of the cells. Average reorientation speed, however, was slower in this case than in OHCs stimulated with an EAEF, suggesting a significant effect of the direction of the electrical field. Intriguingly, the decrease in average reorientation speed was significant only in the apical region of patch-clamped cells (Fig. 5 *B*), whereas peak reorientation speeds were not affected (results not shown).

Microdomain dynamics depends on cholesterol levels in the plasma membrane and on integrity of the cytoskeleton

Treatment of OHCs with MbCD or CWS, which deplete and increase cholesterol in cell membranes, respectively, or with Y27632, which disrupts the cytoskeleton, has region-dependent effects on microdomain rotation (Fig. 6 *A*). In OHCs exposed to MbCD, the average microdomain reorientation speed decreased with respect to control at the basal pole, whereas other regions were unaffected. CSW and Y27632, in contrast, induced significant decreases in

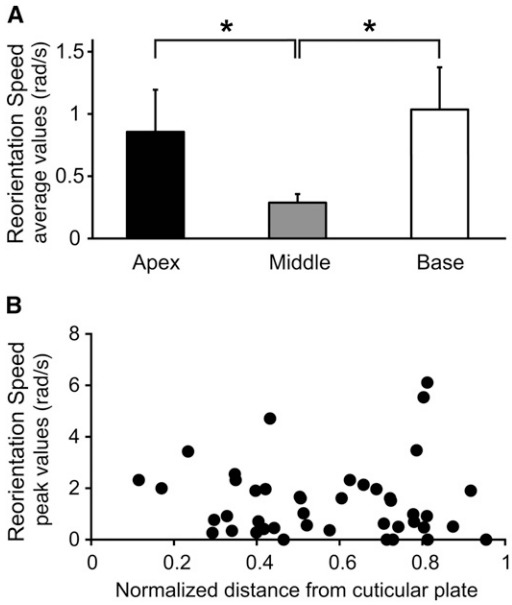

FIGURE 4 MS displacement vectors reorientate with region-dependent average speed but region-independent peak speed. (*A*) Average reorientation speeds were higher at the apical (0.86 ± 0.22 rad/s) and basal (1.05 ± 0.21 rad/s) regions than at the midregion (0.29 ± 0.15 rad/s) of the cells. (*B*) Peak values of reorientation speed, in contrast, were similar in the three regions.

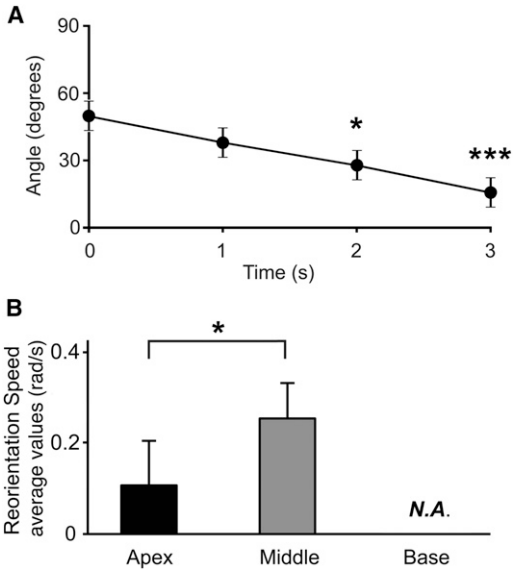

FIGURE.5 MS displacement vectors reorientate with region-dependent average speed in patch-clamped OHCs. (*A*) In response to whole-cell patch clamp stimulation, the average angular distribution of MS (n = 12) displacement vectors decreased progressively, indicating better alignment with the cell longitudinal axes. Alignment was statistically significant 2 s after the start of stimulation and very significant at 3 s (average angles with respect to the cell longitudinal axes: 49.6 ± 8.2° at 0 s, 27.9 ± 6.3° at 2 s (*p ≤ 0.05), and 15.9 ± 4.9° at 3 s, (***p ≤ 0.0009). (*B*) Average reorientation speeds were higher at the midregion (0.25 ± 0.08 rad/s) than at the apical region (0.11 ± 0.10 rad/s) of the cells. Note that values in the midregion were similar in whole-cell and EAEF-stimulated cells (see Fig. 4), whereas values in the apical region were eightfold lower. Thus, the total microdomain average reorientation speed was lower in patch-clamped (0.18 ± 0.09 rad/s) than in EAEF-stimulated cells (0.71 ± 0.17 rad/s). Since patches were always performed at the base of the cells, no reliable data on MS displacement in this region was available. *p ≤ 0.05.

microdomain average reorientation speed at both the apex and the base, without affecting the midregion (Fig. 6 *A*).

Investigating the time dependence of changes in orientation, we found that the angular dispersion at the onset of the treatments was larger at the apex than at the base in MbCD-incubated cells, whereas the reverse was true in cells exposed to CWS (Fig. 6 *B*). We also found differences in the time dependence for changes in orientation between these groups. Whereas angular dispersion decreased significantly during the first second of stimulation and then remained mostly stable during the next second at the apical region of cells treated with MbCD, the decrease in dispersion was more gradual in CWS-treated cells, with no significant difference in rates of change at different time points. In cells exposed to Y27632, time dependence changed at the apical and midregions, becoming gradual at the apex but showing a significantly higher reorganization during the first second of stimulation at the mid- and basal regions of the cells (Fig. 6 *B*).

We also investigated the effect of these treatments on OHC electromotility. The results (Fig. S6) indicate that exposure to MbCD increased the OHC electromechanical response by targeting the apical (cholesterol-rich) region of the cells, whereas CSW and Y27632 decreased it, mostly by their effects on the midregion of the OHC.

DISCUSSION

Our results suggest that MS attach to membrane microdomains, that these microdomains are able to shift and rotate in the plane of the OHC lateral wall, and that their movements are regulated by the membrane skeleton as well as by membrane lipid composition. Since the angular distribution of membrane microdomains, as reported here, and that of cytoskeletal microdomains, as reported by Holley and co-workers (20), are similar and congruent with the axial diffusion angle of lipids in the OHC plasma membrane as measured by fluorescence recovery after photobleaching (23) (Fig. S7), we speculate that MS movements likely reflect the general dynamics of the lateral wall of OHCs, including the plasma membrane and the cortical cytoskeleton.

MS as markers of specific lateral-wall microdomains

Previous studies have indicated that some regions of OHC plasma membrane would be very fluid, and lipid mobility would be affected by the membrane skeleton and correlated with the orientation of cytoskeletal microdomains (23,34,35), whereas others have suggested the existence of

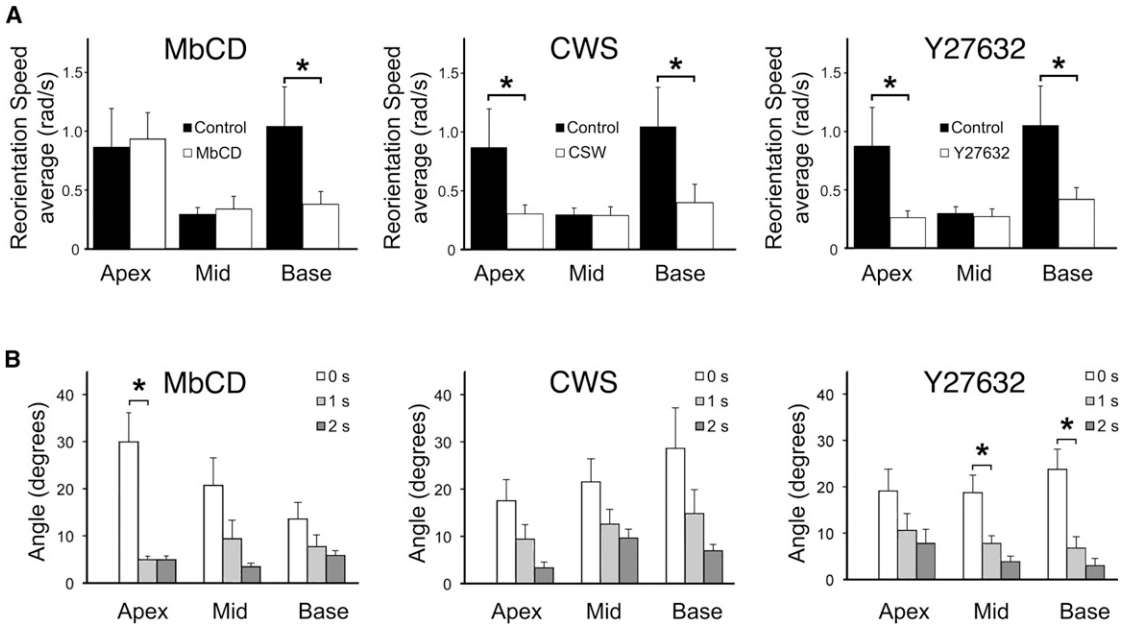

FIGURE 6 Cholesterol levels and cytoskeleton integrity regulate microdomain dynamics. (*A*) Microdomain average reorientation speed at the apex was similar for MbCD-treated and control OHCs and in both cases was significantly higher than at the midregion ($p \leq 0.02$). In contrast, a significant decrease was observed at the basal region in MbCD cells with respect to control cells (0.38 ± 0.20 rad/s vs. 1.05 ± 0.21 rad/s, $p < 0.03$). CSW induced a significant decrease in average reorientation speed at both the apex (0.30 ± 0.15 rad/s vs. 0.86 ± 0.18 rad/s in control, $p \leq 0.03$) and the base (0.40 ± 0.23 rad/s vs. 1.05 ± 0.21 rad/s in control, $p \leq 0.02$), whereas no effects were observed at the midregion (0.28 ± 0.12 rad/s vs. 0.29 ± 0.15 rad/s, NS). Y27632 decreased average reorientation speed at the apex (0.26 ± 0.18 rad/s vs. 0.86 ± 0.18 rad/s in control, $p \leq 0.03$) and the base (0.42 ± 0.24 rad/s vs. 1.05 ± 0.21 rad/s in control, $p \leq 0.05$), but not at the midregion (0.27 ± 0.16 rad/s vs. 0.29 ± 0.15 rad/s in control). (*B*) At 0 s, angular dispersion was bigger at the apex ($29.96 \pm 3.81°$) than at the base ($13.59 \pm 4.57°$) in MbCD-exposed cells but bigger at the base (28.67 ± 5.19 degrees) than at the apex (17.56 ± 3.43 degrees) in CWS-exposed cells. Differences between MbCD and CWS cells were significant at the apex and base, but not at the midregion. Cells exposed to Y27632 showed no difference in angular dispersion with respect to the control condition at 0 s, but time dependence changed at the apical region and midregion, becoming gradual at the apex but showing a higher reorganization during the first second of stimulation at the midregion of the cells.

low-fluidity, gel-like areas in the plasma membrane congruent with the size and distribution of cytoskeletal microdomains (24). We were not able to detect significant drifts in MS attached to nonstimulated OHCs, which supports the idea that they are not influenced by fast lateral diffusion of lipids. In electrically stimulated OHCs, in contrast, MS movement followed, cycle by cycle, the stimulus and changes in the shape of the cells, suggesting that they were strongly attached to the plasma membrane. Thus, we speculate MS movements reflect precisely the movement of specific lateral wall areas (microdomains) to which they are attached. Although we consider microdomains in the OHC lateral wall as pre-existent structures, we cannot rule out the possibility that MS strong attachment to the plasma membrane changes the local organization of the bilayer and the underlying cytoskeleton generating MS-induced microdomains. The following discussion is valid in either case.

Displacement of OHC microdomains in response to osmotic challenge

The response of free-floating OHCs to osmotic challenge was, as expected from a fluid-filled object with anisotropic elastic walls, contraction or elongation around a center of mass located somewhere in the middle of the object. That MS responded accordingly supports the idea that they do not move at random but follow membrane deformations. Moreover, MS trajectories suggest that microdomains at the midregion of the cells move in a wider range of directions than microdomains at the apical or basal pole, a result consistent with a structural reorganization in the midregion to accommodate microdomains moving toward the central plane of the OHCs. In agreement with data from Wada and co-workers (30), we found minimal local deformation in the apical pole of the OHCs, but our data do not support their conclusion that local deformations are constant and uniform in the rest of the OHC lateral wall. We speculate that microdomains at the midregion of the OHCs could be smaller than at the cell's poles and immersed in a region of the plasma membrane with different fluidity. This idea is consistent with experiments with diamide, a drug that affects the cortical cytoskeleton by cross-linking spectrin without apparent effects on actin (36). OHCs exposed to 1 mM diamide yield easily to stretch, showing significant bigger deformation at the midregion than at the poles of the cells (18).

Changes in OHC length and electromotile amplitude are region-dependent

Stimulation with an EAEF induced slow motile responses, with OHC shortening by ~2% in 3 s. Interestingly, length changes in the basal region started later and were significantly less pronounced than in the apical region and midregion. This response could be associated with the low expression of motor proteins (37,38) and differences in lipid composition (39) in the basal pole of the OHCs, as well as with possible structural and functional differences in the cortical cytoskeleton and other cellular structures in this region of the cells (40).

Electromotile amplitude increased from ~1% to ~2.5% of total cell length in the first 2 s of stimulation, reaching its maximum value faster in the apical than in the midregion (Fig. 2 *B*). Regional differences could be associated with differences in motor distribution, an idea supported by measurements of gating current magnitudes, which suggest that the true motor distribution pattern would be different in the midregion than in the poles of the cells (41). These regional differences could also be related to differences in lipid composition, since prestin conformational changes would be maximal in the region with the least cholesterol (42,43). The increase in electromotile amplitude over time, on the other hand, might be explained by the known progressive increase in OHC turgor induced by electrical stimulation (28,33). If that were the case, we should expect that increasing cell turgor would result in the disappearance of this response. In hypo-osmotically challenged cells, however, we observed the same behavior, although electromotile amplitude was initially lower, required >3 s to reach its maximum value, and had a final value significantly higher (~3–3.5% of total cell length) than that measured in control cells (Fig. S4). These results suggest that cell turgor was not a major cause of the observed initial low electromotile amplitude and its increase during the first seconds of stimulation. Another possible explanation could be related to the fast amplificatory shift reported by Santos-Sacchi et al., a phenomenon presumably associated with rapid (in the millisecond to second range) changes in membrane tension that shift the electromotility operating point (44). Although this is clearly a possibility, the question remains as to the cause of these rapid changes in tension in the OHC lateral plasma membrane. Whereas Santos-Sacchi and co-workers suggested that the molecular motors themselves might induce these changes in tension, possibly through alterations of anion binding affinity, a novel explanation based on microdomain reorientation would be consistent with those ideas and with the results of this study.

Rotation of OHC microdomains

Since actin filaments are practically inextensible and spectrin tetramers are easily deformable, potential conformational changes in prestin motor proteins embedded in the plasma membrane would result in MS movements in a direction perpendicular to actin filaments (Fig. 7). Thus, our results indicating that initial MS trajectories had a variable orientation are consistent with the variable orientation of actin filaments along the OHC lateral wall (20,45).

Electrical stimulation induced fast reorientation of MS displacement vectors, which became aligned with the longitudinal axes of the OHCs. Of greatest importance is the fact that the alignment was lost after periods of 5 min or longer

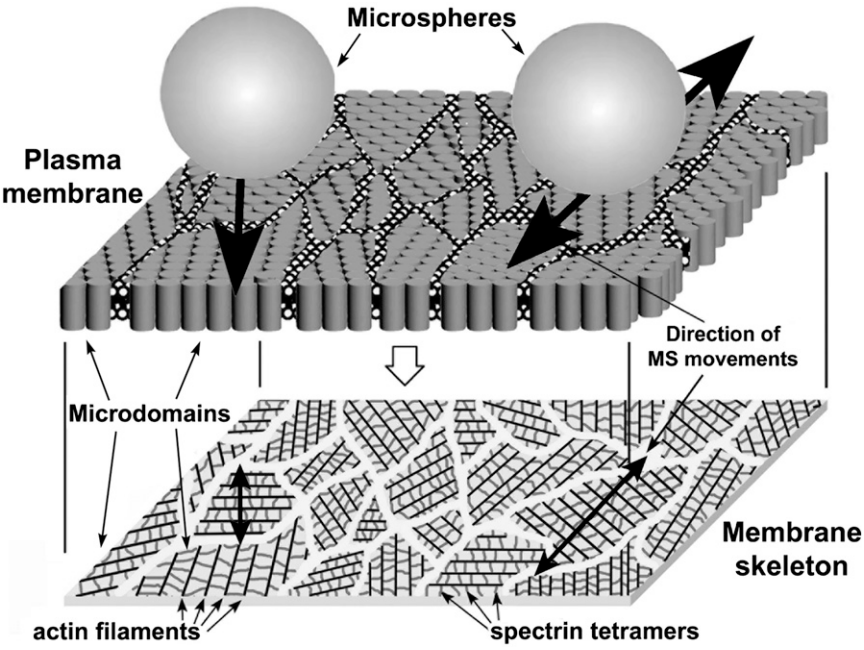

FIGURE 7 Schematic diagram (not to scale) depicting plasma membrane and cytoskeletal microdomains, as well as the electromotility-induced movement of MS attached to particular microdomains. Gray cylinders embedded in the lipidic bilayer represent prestin and prestin-associated proteins, clusters of which define the membrane microdomains. The interdomain regions are represented as lipid-only areas for clarity, but they could contain different protein populations, including prestin, that are not associated with microdomains. In the membrane skeleton, in turn, near-parallel black lines represent actin filaments, whereas spectrin tetramers are shown as short traces connecting actin filaments; the direction of actin filaments varies among different microdomains. Note that the direction of the movements induced by an EAEF in microspheres attached to particular plasma membrane microdomains (*arrows*) would be perpendicular to the direction of the actin filaments in the corresponding cytoskeletal microdomain.

without electrical stimulation, which indicates that microdomains are naturally free to move in the plane of the OHC lateral wall to reach or return to their distribution of equilibrium. The lower average reorientation speed observed in patch-clamped cells suggests that microdomains will always tend to align with the longitudinal axis in motile cells, but reorientation speed might be regulated by varying the direction of the electrical field. However, we cannot rule out the possibility that the slower microdomain re-orientation speed observed in patch clamped cells may be due to washing out important cell signaling molecules involved in this process. Nevertheless, since microdomains in the lateral wall of cochlear OHCs would be able to shift and rotate in both the presence and absence of an electrical field, we propose that they would be able to shift and rotate in physiological conditions under the influence of specific cellular signals and mechanisms to optimize the mechanical response of the system.

How the direction of the electrical field could affect microdomain reorientation is an intriguing question. We speculate that cytoskeletal constraints could induce a deformation of the motor proteins in the particular direction of the spectrin tetramers in each microdomain, leading to charge separation and generation of a dipolar momentum in every motor molecule. The electrical field could induce torque about the center of each dipole, causing the dipole to rotate and thus aligning the complete microdomain with the electrical field. In fact, a similar dipolar momentum could be generated in each spectrin molecule in the cortical cytoskeleton, and microdomain rotation might result from the contribution of both mechanisms working in synchrony. It should be emphasized, however, that microdomain reorientation is not necessarily driven directly by electric field forces. As indicated by whole-cell patch-clamp experiment, when no unidirectional extracellular electric field is present, it is possible that cycles of contraction/elongation would similarly align the microdomains with the longitudinal axis of the cells due to inherent constraints.

An interesting point is the characterization of the particular trajectories followed by the MS during electrical stimulation and the reorientation process. This, however, is not a trivial problem, and we did not try to cover it in this study. We are currently working to develop a way to perform automatically, frame by frame in tens of thousands of frames, the corrections associated with relative MS position, cell movement, and changes in curvature, as well as the interactions of each particular microdomain with neighboring microdomains, to characterize these trajectories.

Microdomain reorientation provides a straightforward explanation for the observed fast increase in electromotile amplitude observed here (Fig. 3 *B*) as well as in past experiments (28). Microdomain alignment would maximize the longitudinal component of the force generated at the plasma membrane by the motor molecules. Moreover, microdomain reorientation might result in a rapid change in membrane tension, resulting in the additional amplificatory shift reported by Santos-Sacchi et al. (44), whereas an increase in turgor might result in a different amplificatory shift with a longer time course, probably related to improved effectiveness of the hydraulic communication of motor force.

Effects of cholesterol and cytoskeleton integrity on MS dynamics

Our results indicate that microdomain reorientation proceeded faster in the apical and basal poles than in the midregion of OHCs. Regional differences may be a consequence of underlying differences in composition and structure of the plasma membrane and the actin-based cortical lattice. It is known, for example, that the density of prestin, the motor molecule in the OHC plasma membrane, is lower in the basal pole than in the lateral wall (37,38), and that cholesterol is less abundant in the midregion than in the apical and basal regions (39).

Changes in cholesterol levels affected microdomain dynamics in a region-dependent manner. Since physical properties of membranes suggest that increasing membrane cholesterol increases membrane rigidity (42,46), we can speculate that the CWS-induced decrease in microdomain reorientation in the apical region of the OHCs could be associated with a decrease in membrane fluidity. Since cholesterol may exert its effect by directly binding to membrane proteins, affecting protein conformation and dynamics (47), we speculate that the low density of motor proteins in the basal pole of the OHCs could facilitate their interaction with cholesterol, explaining the decrease in microdomain reorientation induced by both CWS and MbCD. In a similar way, the high density of motor proteins might be interfering with the effects of CWS and MbCD in the midregion of the cells. Recent results indicating that cholesterol depletion could strengthen interaction between the plasma membrane and cytoskeleton, whereas cholesterol augmentation would weaken this interaction (48), offer an alternate explanation, not necessarily incompatible with the previous one. The strong interaction between plasma membrane and cytoskeleton in the midregion of the cells would not be essentially affected by CWS or MbCD, whereas a CWS-induced weakening of this interaction at the apex would lead to a significant decrease in microdomain reorientation rate in this region. At the OHC base, in contrast and for a reason still unknown, any change in the weak interaction between plasma membrane and cytoskeleton would result in a decrease in microdomain reorientation speed. Clearly, more work is necessary to understand the dynamics of the microdomains in the lateral wall of OHCs.

CONCLUSIONS

The movements of MS attached to the OHC lateral wall suggest that it would be organized as a mosaic of

microdomains with orientations defined by the direction of actin filaments in the membrane skeleton. These microdomains would be able to shift and rotate in the plane of the OHC lateral wall with a dynamic tightly regulated by membrane lipid composition and the cortical cytoskeleton. These results confirm and extend those of previous studies supporting the modular organization of the lateral wall of cochlear OHCs.

SUPPORTING MATERIAL

Seven figures and two movies are available at http://www.biophysj.org/biophysj/supplemental/S0006-3495(12)05075-8.

We thank Dr. Laurel M. Fisher for assistance with statistical analysis and Dr. Zahara Jaffer for critically reading the manuscript. The content of this article is solely the responsibility of the authors and does not necessarily represent the official views of the National Institute on Deafness and Other Communication Disorders or those of House Research Institute. The authors declare no existing or potential conflict of interest.

This work was made possible by grants R01DC10146 and P30DC006276 from the National Institute on Deafness and Other Communication Disorders, National Institutes of Health, and the support of House Research Institute.

REFERENCES

1. Jacobson, K., O. G. Mouritsen, and R. G. Anderson. 2007. Lipid rafts: at a crossroad between cell biology and physics. *Nat. Cell Biol.* 9:7–14.
2. Lillemeier, B. F., J. R. Pfeiffer, …, M. M. Davis. 2006. Plasma membrane-associated proteins are clustered into islands attached to the cytoskeleton. *Proc. Natl. Acad. Sci. USA.* 103:18992–18997.
3. Lim, D. J., and F. Kalinec. 1998. Cell and molecular basis of hearing. *Kidney Int. Suppl.* 65:S104–S113.
4. Frank, G., W. Hemmert, and A. W. Gummer. 1999. Limiting dynamics of high-frequency electromechanical transduction of outer hair cells. *Proc. Natl. Acad. Sci. USA.* 96:4420–4425.
5. Grosh, K., J. Zheng, …, A. L. Nuttall. 2004. High-frequency electromotile responses in the cochlea. *J. Acoust. Soc. Am.* 115:2178–2184.
6. Ashmore, J. 2008. Cochlear outer hair cell motility. *Physiol. Rev.* 88:173–210.
7. Matsumoto, N., R. Kitani, …, F. Kalinec. 2010. Pivotal role of actin depolymerization in the regulation of cochlear outer hair cell motility. *Biophys. J.* 99:2067–2076.
8. Matsumoto, N., R. Kitani, and F. Kalinec. 2011. Linking LIMK1 deficiency to hyperacusis and progressive hearing loss in individuals with Williams syndrome. *Commun. Integr. Biol.* 4:208–210.
9. Zha, D., F. Chen, …, A. L. Nuttall. 2012. In vivo outer hair cell length changes expose the active process in the cochlea. *PLoS ONE.* 7:e32757.
10. Ramamoorthy, S., and A. L. Nuttall. 2012. Outer hair cell somatic electromotility in vivo and power transfer to the organ of Corti. *Biophys. J.* 102:388–398.
11. Chen, F., D. Zha, …, A. L. Nuttall. 2011. A differentially amplified motion in the ear for near-threshold sound detection. *Nat. Neurosci.* 14:770–774.
12. Kalinec, F., M. C. Holley, …, B. Kachar. 1992. A membrane-based force generation mechanism in auditory sensory cells. *Proc. Natl. Acad. Sci. USA.* 89:8671–8675.
13. Zheng, J., W. Shen, …, P. Dallos. 2000. Prestin is the motor protein of cochlear outer hair cells. *Nature.* 405:149–155.
14. Johnson, S. L., M. Beurg, …, R. Fettiplace. 2011. Prestin-driven cochlear amplification is not limited by the outer hair cell membrane time constant. *Neuron.* 70:1143–1154.
15. Gulley, R. L., and T. S. Reese. 1977. Regional specialization of the hair cell plasmalemma in the organ of Corti. *Anat. Rec.* 189:109–123.
16. Forge, A. 1991. Structural features of the lateral walls in mammalian cochlear outer hair cells. *Cell Tissue Res.* 265:473–483.
17. Reference deleted in proof.
18. Kalinec, F., and B. Kachar. 1995. Structure of the electromechanical transduction mechanism in mammalian outer hair cells. *In* Active Hearing. Å. Flock, D. Ottoson, and M. Ulfendahl, editors. Elsevier Science, Oxford, United Kingdom. 179–191.
19. Santos-Sacchi, J. 2002. Functional motor microdomains of the outer hair cell lateral membrane. *Pflugers Arch.* 445:331–336.
20. Holley, M. C., F. Kalinec, and B. Kachar. 1992. Structure of the cortical cytoskeleton in mammalian outer hair cells. *J. Cell Sci.* 102:569–580.
21. Leonova, E. V., and Y. Raphael. 1999. Application of a platinum replica method to the study of the cytoskeleton of isolated hair cells, supporting cells and whole mounts of the organ of Corti. *Hear. Res.* 130:137–154.
22. Wada, H., K. Kimura, …, T. Kobayashi. 2004. Imaging of the cortical cytoskeleton of guinea pig outer hair cells using atomic force microscopy. *Hear. Res.* 187:51–62.
23. de Monvel, J. B., W. E. Brownell, and M. Ulfendahl. 2006. Lateral diffusion anisotropy and membrane lipid/skeleton interaction in outer hair cells. *Biophys. J.* 91:364–381.
24. Zhang, M., and F. Kalinec. 2002. Structural microdomains in the lateral plasma membrane of cochlear outer hair cells. *J. Assoc. Res. Otolaryngol.* 3:289–301.
25. Matsumoto, N., and F. Kalinec. 2005. Extraction of prestin-dependent and prestin-independent components from complex motile responses in guinea pig outer hair cells. *Biophys. J.* 89:4343–4351.
26. Matsumoto, N., and F. Kalinec. 2005. Prestin-dependent and prestin-independent motility of guinea pig outer hair cells. *Hear. Res.* 208:1–13.
27. Kitani, R., and F. Kalinec. 2011. Investigating outer hair cell motility with a combination of external alternating electrical field stimulation and high-speed image analysis. *J. Vis. Exp.* 53:2965.
28. Kitani, R., S. Kakehata, and F. Kalinec. 2011. Motile responses of cochlear outer hair cells stimulated with an alternating electrical field. *Hear. Res.* 280:209–218.
29. Adachi, M., and K. H. Iwasa. 1997. Effect of diamide on force generation and axial stiffness of the cochlear outer hair cell. *Biophys. J.* 73:2809–2818.
30. Wada, H., H. Usukura, …, K. Ikeda. 2001. Distribution of protein motors along the lateral wall of the outer hair cell. *Hear. Res.* 162:10–18.
31. Rajagopalan, L., J. N. Greeson, …, W. E. Brownell. 2007. Tuning of the outer hair cell motor by membrane cholesterol. *J. Biol. Chem.* 282:36659–36670.
32. Kakehata, S., and J. Santos-Sacchi. 1996. Effects of salicylate and lanthanides on outer hair cell motility and associated gating charge. *J. Neurosci.* 16:4881–4889.
33. Santos-Sacchi, J. 1991. Reversible inhibition of voltage-dependent outer hair cell motility and capacitance. *J. Neurosci.* 11:3096–3110.
34. Oghalai, J. S., T. D. Tran, …, W. E. Brownell. 1999. Transverse and lateral mobility in outer hair cell lateral wall membranes. *Hear. Res.* 135:19–28.
35. Oghalai, J. S., H.-B. Zhao, …, W. E. Brownell. 2000. Voltage- and tension-dependent lipid mobility in the outer hair cell plasma membrane. *Science.* 287:658–661.
36. Becker, P. S., C. M. Cohen, and S. E. Lux. 1986. The effect of mild diamide oxidation on the structure and function of human erythrocyte spectrin. *J. Biol. Chem.* 261:4620–4628.

37. Belyantseva, I. A., H. J. Adler, …, B. Kachar. 2000. Expression and localization of prestin and the sugar transporter GLUT-5 during development of electromotility in cochlear outer hair cells. *J. Neurosci.* 20:RC116.

38. Mahendrasingam, S., M. Beurg, …, C. M. Hackney. 2010. The ultrastructural distribution of prestin in outer hair cells: a post-embedding immunogold investigation of low-frequency and high-frequency regions of the rat cochlea. *Eur. J. Neurosci.* 31:1595–1605.

39. Nguyen, T. V., and W. E. Brownell. 1998. Contribution of membrane cholesterol to outer hair cell lateral wall stiffness. *Otolaryngol. Head Neck Surg.* 119:14–20.

40. Lim, D. J. 1986. Functional structure of the organ of Corti: a review. *Hear. Res.* 22:117–146.

41. Takahashi, S., and J. Santos-Sacchi. 2001. Non-uniform mapping of stress-induced, motility-related charge movement in the outer hair cell plasma membrane. *Pflügers Arch.* 441:506–513.

42. Sfondouris, J., L. Rajagopalan, …, W. E. Brownell. 2008. Membrane composition modulates prestin-associated charge movement. *J. Biol. Chem.* 283:22473–22481.

43. Brownell, W. E., S. Jacob, …, A. Fridberger. 2011. Membrane cholesterol modulates cochlear electromechanics. *Pflugers Arch.* 461:677–686.

44. Santos-Sacchi, J., E. Navarrete, and L. Song. 2009. Fast electromechanical amplification in the lateral membrane of the outer hair cell. *Biophys. J.* 96:739–747.

45. Holley, M. C. 1996. Outer hair cell motility. *In* The Cochlea. P. Dallos, A. N. Popper, and R. R. Fay, editors. Springer, New York. 386–434.

46. Needham, D., and R. S. Nunn. 1990. Elastic deformation and failure of lipid bilayer membranes containing cholesterol. *Biophys. J.* 58:997–1009.

47. Levic, S., and E. N. Yamoah. 2011. Plasticity in membrane cholesterol contributes toward electrical maturation of hearing. *J. Biol. Chem.* 286:5768–5773.

48. Khatibzadeh, N., S. Gupta, …, B. Anvari. 2012. Effects of cholesterol on nano-mechanical properties of the living cell plasma membrane. *Soft Matter.* 8:8350–8360.